RADIATION RESEARCH **179**, 313–322 (2013)
0033-7587/13 $15.00

DOI: 10.1667/RR3179.1

# Room Temperature Radiation Products in Trehalose Single Crystals: EMR and DFT Analysis

Hendrik De Cooman,[a,b] Mihaela Adeluta Tarpan,[a] Henk Vrielinck,[a] Michel Waroquier[b] and Freddy Callens[a,1]

[a] *Department of Solid State Sciences, Ghent University, Krijgslaan 281-S1, B-9000 Gent, Belgium; and* [b] *Center for Molecular Modeling, Ghent University, Technologiepark 903, B-9052 Zwijnaarde, Belgium*

**De Cooman, H., Tarpan, M. A., Vrielinck, H., Waroquier, M. and Callens, F. Room Temperature Radiation Products in Trehalose Single Crystals: EMR and DFT Analysis. *Radiat. Res*. 179, 313–322 (2013).**

**Radicals generated in trehalose single crystals by X radiation at room temperature were investigated by electron paramagnetic resonance (EPR), electron nuclear double resonance (ENDOR) and ENDOR-induced EPR measurements, together with periodic density functional theory calculations. In the first days after irradiation, three radical species (I1, I2 and I3) were detected, two of which (I1 and I2) dominate the EPR spectrum and could be identified as H-abstracted species centered at C3′ (I1) and C2 (I2), the latter with additional formation of a carbonyl group at C3. Annealing the sample at 40°C for 3 days or storing it in ambient conditions for three months resulted in another, more stable EPR spectrum. Two major species could be characterized in this stage (S1 and S2), only one of which was tentatively identified as an H-abstracted, C2-centered species (S1). Our findings disagree with a previous EPR study [Gräslund and Löfroth (*23*)] on several accounts. This work stresses the need for caution when interpreting composite EPR spectra and thermally induced spectral changes of radiation-induced species, even in these relatively simple carbohydrates. It also provides further evidence that the pathways for radiation damage critically depend on the specific conformation of a molecule and its environment, but also that carbonyl group formation is a common process in the radiation chemistry of sugars and related compounds.** 

## INTRODUCTION

In the last few years, radicals induced by X rays in single crystals of various monosaccharides (*1–6*), polysaccharides (*7–12*) and sugar phosphates (*13–14*) have been investigated in detail in our laboratories using both electron magnetic resonance (EMR) experiments [electron paramagnetic resonance (EPR), electron nuclear double resonance (ENDOR) and ENDOR-induced EPR (EIE)] and advanced density functional theory (DFT) calculations. The main goal of this research is to improve the understanding of the radiation chemistry in solid carbohydrates, which is important from a fundamental point of view and may help to elucidate the direct radiation effect in the sugar units of the DNA helix. The latter is of considerable importance as sugar radicals are the main precursors for double-strand breaks, the most harmful form of DNA damage with respect to biological consequences (*15, 16*). Our main research objectives include uncovering general principles in the radiation-induced reactions and understanding the selectivity of radical formation in these materials. First and foremost, this requires reliable identification of the radicals in a sufficiently large number of materials and at different stages of the post-radiation chemistry. While the more stable products can be investigated after irradiation at room temperature, the primary and intermediate species have to be studied using *in situ* irradiation at lower temperatures (*17*). Such studies can also provide interesting information (e.g., with respect to the compositeness of the EPR signal) in the context of using sugars for (emergency) dosimetry (*10, 18*).

The radiation products in sucrose (a disaccharide consisting of one glucose and one fructose unit, Fig. 1A) were studied in detail both after room temperature irradiation (*7–10*) and 10 K *in situ* irradiation (*11*). To evaluate the extent to which the findings of these studies can be generalized, we have undertaken a series of analogous investigations on structurally similar disaccharides. We recently published two articles on radiation defects in trehalose (consisting of two glucose units, Fig. 1B) after irradiation at 10 K (*19*) and 77 K (*20*), which extended previous work in the literature (*21, 22*). The current work focuses on the radiation products after room-temperature irradiation.

Trehalose single crystals X irradiated at room temperature have been studied in the past with EPR by Gräslund and

*Editor's note*. The online version of this article (DOI: 10.1667/RR3179.1) contains supplementary information that is available to all authorized users.

[1]Address for correspondence: Department of Solid State Sciences, Ghent University, Krijgslaan 281-S1, B-9000 Gent, Belgium; e-mail: Freddy.Callens@ugent.be.

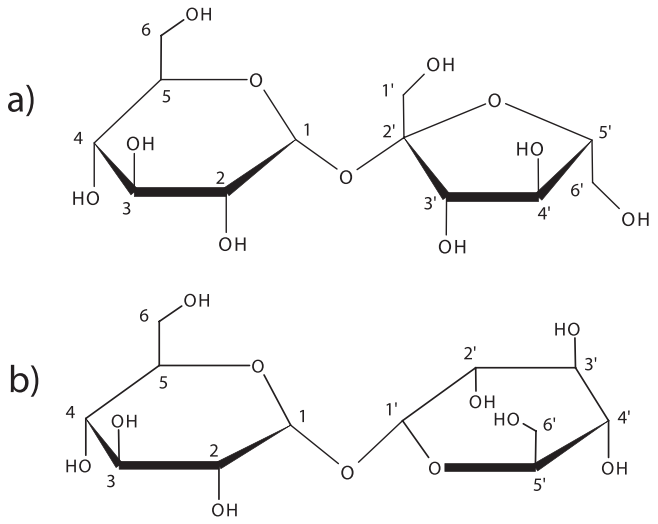


**FIG. 1.** Chemical structures of sucrose (a) and trehalose (b).

Löfroth (*23*). Immediately after irradiation, they observed an EPR spectrum dominated by a triplet with a 3 mT splitting and a 1:2:1 intensity ratio, which they attributed to C3- and C3′-centered radicals (''species A''), assuming that radical formation occurs with equal probability in each of the monosaccharide units. Irradiation at 77 K was reported to result in similar spectra, which the authors assumed to originate from the same radical species. They observed a complete change of the EPR spectrum after 3 months at room temperature. The final EPR spectrum (stable for at least 1 year according to Gräslund and Löfroth) was tentatively attributed to two radical species, centered at C2 and C2′ and resulting from a β-elimination reaction of species A, with carbonyl group formation at C3 and C3′, respectively. Hyperfine (HF) tensors were not determined and the structural identifications were based on the magnitude of the isotropic HF interactions, the Heller-McConnell relation (*24, 25*) and chemical intuition. In the present work the radiation products after room-temperature irradiation were investigated more in detail using ENDOR and EIE measurements (in addition to EPR measurements) and periodic DFT calculations. These revealed the presence of additional species and provided more accurate EMR parameters, which led to corrections to the structural identifications in some cases.

## MATERIALS AND METHODS

Trehalose dihydrate has an orthorhombic ($P2_12_12_1$) crystal structure with four trehalose and eight water molecules per unit cell, and lattice parameters a = 1.223 nm, b = 1.789 nm and c = 0.7596 nm (*26*). The procedures for crystal growth have been described elsewhere (*19*), as well as the procedures for the orientation and irradiation of single crystals and extraction of the HF tensors from the ENDOR angular variations and simulations (*7*). Samples were X irradiated (60 keV) to a dose of approximately 30 kGy at room temperature. Otherwise, the EMR measurements were performed on a Q-band spectrometer (Bruker Elexsys E500, equipped with a CF935 cryostat, Oxford Instruments) at 50 K. Some X-band EPR and ENDOR experiments were conducted on a Bruker ESP300E spectrometer with an ESR10 cryostat (Oxford Instruments). The microwave frequency was measured using an EIP 548B or HP 5350B frequency counter, respectively. The ENDOR signals could not be detected at room temperature and had quite low intensity at liquid $N_2$ temperature. Cooling below 50 K did not yield a considerable improvement in S/N ratio. EPR spectra recorded at room temperature and 50 K exhibited the same features with limited differences in relative line intensities. ENDOR angular variations were obtained over 100° with 5° intervals in the ab, bc and ac planes. At every orientation, the ENDOR spectra were recorded for at least two different magnetic field values.

The Schonland ambiguity (*27, 28*), an ambiguity in the anisotropic part of the HF tensor, was eliminated for the HF1(I1), HF2(I1) and HF1(S1) tensors by measurements in a slightly skewed plane (polar angles $\theta = 98°$ and $\varphi = -2°$) instead of the *bc* plane in the Q-band, and in a fourth skewed plane (polar angles $\theta = 86°$ and $\varphi = 63°$) in the X-band. However, these data did not allow the elimination of the Schonland ambiguity for the other HF tensors due to the combination of weak ENDOR line intensities and fourfold site splitting in the additional rotation planes (as opposed to only twofold site splitting in the ab, bc and ac planes). The tensors with the most axial principal values are reported in this work, and the Schonland-conjugate forms were calculated [following the procedure in ref. (*28*)] and are listed in Supplementary Table S1 (http://dx.doi.org/10.1667/RR3179.1.S1). We systematically considered both forms in our search for model structures (when comparing principal directions with pristine crystal directions or an HF tensor with one that was DFT-calculated). However, this did not reveal other relevant radical models, neither did it result in a considerable improvement for any of the proposed models. In this respect the Schonland ambiguity does not have implications for the discussions on radical identities in this work.

The computational protocol used for the DFT calculations has been reported in our previous publications on radiation defects in trehalose (*19, 20*). Geometry optimizations and HF tensor calculations (*29*) were performed in an advanced all electron scheme with periodic boundary conditions on a crystal unit cell (four trehalose and eight water molecules) using the Gaussian-augmented plane-wave (GAPW) method (*30*) (plane-wave cutoff of 250 Ry, TZV2P basis set) and a BLYP functional (*31, 32*) in the CP2K software suite (*33*). Periodic calculations provided the most natural and complete approach for simulating the crystal lattice environment and were, especially with respect to geometry optimizations, superior to computational schemes in which the lattice was not or only partially taken into account. Since the EPR parameters of a radical strongly depend on its geometry, the use of periodic boundary conditions was also crucial in this respect.

The experimental crystallographic structure of the lattice served as starting point for the various radical species on which we performed DFT calculations. In addition, only relatively simple alterations to this structure were considered. It is important to note that after room-temperature irradiation, the observed radicals may be the end product of complicated reaction chains and there may be significant (diamagnetic) damage to the lattice, in addition to the (paramagnetic) radicals that can be observed directly in our magnetic resonance experiments. These basic limitations of the DFT modeling study presented in the current work should be kept in mind. Nevertheless, using the pristine crystal lattice as starting point is a highly useful approach as well as for investigating radicals induced at room temperature, which is apparent from the results in this and previous (*8, 9*) studies in our laboratories.

Trehalose is orthorombic with four molecules per unit cell (four symmetry-related sites), but the HF tensors for only one of these sites are reported for a given radical. Also, EMR experiments cannot discern between sites related by inversion symmetry. Therefore, care should be taken when comparing experimental HF principal directions with those that are calculated or with pristine crystal directions. In this work, we have always performed (orthorombic and inversion)

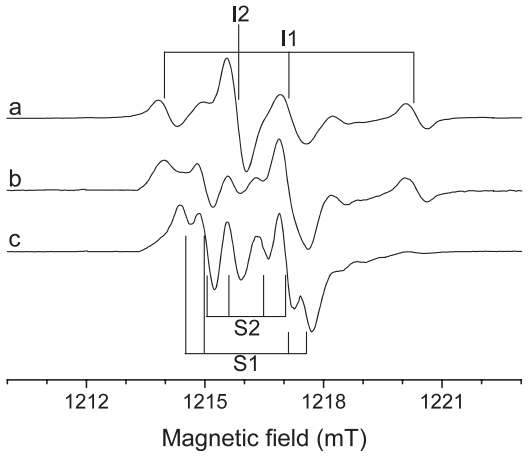


**FIG. 2.** Evolution of the Q-band EPR spectrum (amplitude-normalized) of a room-temperature irradiated trehalose single crystal for B // <b>. The EPR spectra were recorded (a) 1 day after irradiation, (b) after storing the crystals for 2 days at 40°C and (c) after storing the crystal for a third day at 40°C.

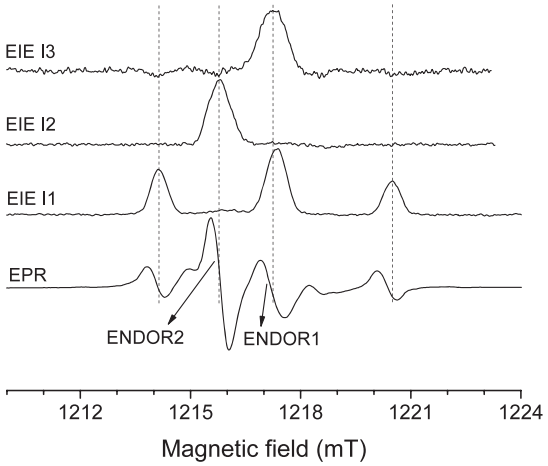


**FIG. 3.** Q-band EPR and EIE spectra of a trehalose single crystal for B // <b> 1 day after room temperature X irradiation. The magnetic field positions at which the ENDOR spectra of Fig. 5 were recorded are indicated by arrows.

symmetry operations on the tensors such that the smallest deviation angle is obtained for the $\bar{V}_{max}$ principal direction (associated with the largest principal HF value $A_{max}$).

## EXPERIMENTAL RESULTS AND DISCUSSION

### *Time Evolution and Decomposition of the EPR Spectra*

The EPR spectra of trehalose single crystals irradiated at room temperature undergo slow but continuous changes during the first months after irradiation. After 3 months, a stable state is reached, with quite different spectral characteristics than initially observed. The same conversion is observed over a timespan of only 3 days when the sample is stored at 40°C in a closed oven after irradiation. These findings are in accordance with those reported by Gräslund and Löfroth (*23*). The transformation of the EPR spectrum is shown in Fig. 2 for B // <b>. The first few days after irradiation (keeping the crystal in ambient conditions) are referred to as ''initial'' in this article, while 3 months (3 days if the sample is stored at 40°C) or more after irradiation will be referred to as ''stable''. The species at these two stages will be labeled with 'I' and 'S', respectively.

EPR, ENDOR and EIE experiments showed that the dominant contributions to the initial EPR spectra are a triplet with a 1:2:1 intensity ratio (species I1) and a singlet (species I2). This is illustrated for B // <b> in Fig. 2A and Fig. 3. EPR angular variations show the *g* anisotropy is small for both species and typical of carbon-centered radicals. Due to the limited variation in *g* factor and the composite nature of the EPR spectra (further complicated by hyperfine splittings and broad lines), we were not able to extract reliable *g* tensors. Full EIE angular variations should suffice for this purpose, but are very laborious and have not been carried out here. Nevertheless, our data indicate that the *g* anisotropy is markedly larger for I2 than for I1, which points to partial delocalization of the spin density onto oxygen for I2, e.g., due to a carbonyl group neighboring the radical center (*34*).

Species I1 and I2 have largely decayed after 3 and 2 days, respectively, at 40°C (Fig. 2). Additional measurements revealed that I2 has decayed after less than a week when the sample was stored in ambient conditions. ENDOR signals of a third radical species (I3) were detected during the first day after irradiation, but their S/N ratio was too low for a reliable determination of HF tensors. EIE spectra (Fig. 3, the spectra for B // <b> is given) suggest that I3 only has HF interactions with small isotropic values (<20 MHz) and limited anisotropy (protons at β positions or further away). The I3 ENDOR signals also decayed faster than those of I1 or I2 and the relative concentration of I3 must be small judging by the limited changes in the EPR spectrum during the first day.

The stable EPR spectra are dominated by resonances of two other radical species (S1 and S2). Both have a doublet HF pattern of broad lines at most orientations. However, an additional smaller HF splitting is resolved at some orientations (Figs. 2C and 4). S1 and S2 exhibit limited *g* anisotropy typical of carbon-centered radicals. Determination of the *g* tensors by EIE is even more cumbersome here, considering the rather low ENDOR intensities. In this case, our data is insufficient to determine whether or not the spin density is partially delocalized onto oxygen in these radicals. Careful inspection of ENDOR spectra and additional EIE measurements showed that S1 and S2 are already present in the initial stage, albeit with a markedly lower ENDOR intensity. The EPR signatures of S1 and S2 may therefore account for some of the less dominant features in the initial EPR spectrum, which cannot be attributed to I1, I2 or I3 (Fig. 3).

These observations indicate that the EPR spectral evolution is probably at least in part due to the production

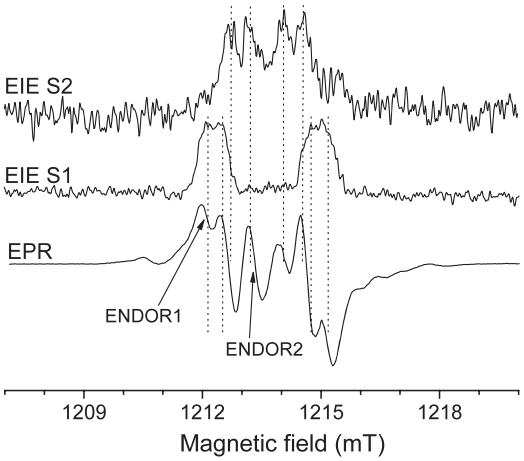


**FIG. 4.** Q-band EPR and EIE spectra of trehalose single crystals after room-temperature X irradiation and annealing at 40°C for 3 days (B // <b>). The magnetic field positions at which the ENDOR spectra of Fig. 8 were recorded are indicated by arrows.

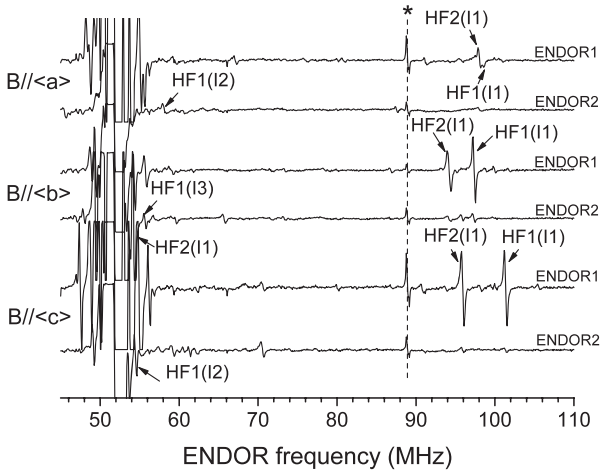


**FIG. 5.** Q-band ENDOR spectra of trehalose single crystals one day after room-temperature X irradiation for the magnetic field along the <a>, <b> and <c> axes. For each orientation, the ENDOR spectra are shown for two different positions in the EPR spectrum, as indicated by arrows for B // <b> in Fig. 3. The signal at 89 MHz (indicated by *) is an artifact.

of the stable species and not only to the decay of the initial species. X-band EPR measurements on trehalose powder shortly after irradiation and after storage for 3 days at 40°C reveal a net radical decay, however, the total intensity (double integral) of the stable EPR spectrum being about 30–50% of that of the initial EPR spectrum. This is in contrast to the findings of Gräslund and Löfroth who reported a constant spin concentration during the spectral changes over a 3-month period (*23*). Possible reasons for this discrepancy may be the differences in storage temperature, wavelength of the ionizing radiation and dose rate.

### *ENDOR and DFT Analysis*

*Initial species*. ENDOR spectra obtained with the magnetic field along the crystal axes are shown in Fig. 5. For four proton HF couplings, sufficient data were gathered from the ENDOR angular variations to determine the corresponding tensors (Fig. 6 and Table 1): two for I1 [(HF1(I1) and HF2(I1)] and two for I2 [(HF1(I2) and HF2(I2)]. As shown in Fig. 5, there are various other ENDOR lines that could not be analyzed because they were observed for only a limited number of orientations. Even if some of them are relatively intense, no clear EIE spectra were obtained. Some likely originate from the stable S1 and S2 species (at 70 and 86 MHz), while lines close to the proton Larmor frequency could be due to weak HF couplings associated with I1, I2 or I3. Yet, other ENDOR lines (around 66, 67 and 80 MHz, in particular) indicate the presence of other (minor) species.

In correspondence with the EIE spectrum shown in Fig. 3, I1 exhibits two typical β-proton HF interactions of similar strength. Their anisotropy is characteristic of nonexchangeable protons (*35, 36*), in accordance with the findings of Gräslund and Löfroth who observed only limited changes in the EPR spectrum of deuterated crystals (*23*). A variety of radical species may exhibit such couplings, those obtained by H abstraction at C2, C3, C4, C5, C2′, C3′, C4′ or C5′ being the most obvious. The $\vec{V}_{max}$ eigenvectors of HF1(I1) and HF2(I1) agree best with the $C_\alpha$—$H_\beta$ directions of the pristine molecule for the C5-, C3′- and C5′-centered species (see Table S2: http://dx.doi.org/10.1667/RR3179.1.S1). The DFT-calculated proton HF tensors of these structures are reported in Supplementary Table S3 (http://dx.doi.org/10.1667/RR3179.1.S1) and clearly favor the C3′-centered species (model $I1_M$ in Fig. 7, HF tensors in Table 2), whereas only one sufficiently large HFC is predicted for the C5-centered species, and the eigenvector deviations are large for the C5′-centered species. Additionally, the overall

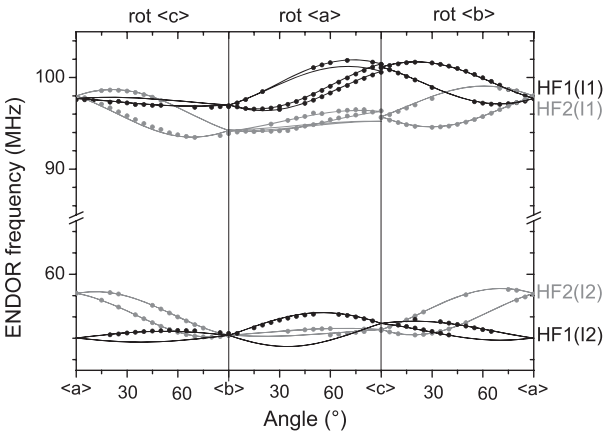


**FIG. 6.** Q-band ENDOR angular variation of proton HF interactions of the initial radical species in room-temperature irradiated trehalose single crystals in the ab, bc and ac planes. The solid circles represent the experimental data of the interactions for which HF tensors were determined and the solid lines are simulations using the HF tensors in Table 1.

**TABLE 1**
**Experimental Proton HF Tensors of the Initial (I1 and I2) and Stable (S1 and S2) Radical Species Generated in Trehalose Single Crystals by X Irradiation At Room Temperature Obtained from Q-Band ENDOR Measurements**

| | | | Principal directions | | |
|---|---|---|---|---|---|
| Radical species | Iso (MHz) | Aniso (MHz) | a | b | c |
| I1 | | | | | |
| HF1 | 94.13 | –5.18 | 0.498 | 0.778 | –0.382 |
| | | –1.73 | 0.813 | –0.572 | –0.104 |
| | | 6.91 | 0.300 | 0.259 | 0.918 |
| HF2 | 88.84 | –5.16 | 0.439 | 0.863 | –0.250 |
| | | –2.11 | 0.301 | –0.403 | –0.864 |
| | | 7.27 | 0.847 | –0.304 | 0.437 |
| I2 | | | | | |
| HF1 | 8.56 | –3.27 | 0.230 | 0.967 | 0.110 |
| | | –2.85 | 0.293 | –0.177 | 0.940 |
| | | 6.12 | 0.928 | –0.184 | –0.324 |
| HF2 | 5.90 | –2.66 | 0.127 | –0.833 | 0.539 |
| | | –1.45 | 0.954 | –0.048 | –0.297 |
| | | 4.11 | 0.273 | 0.552 | 0.788 |
| S1 | | | | | |
| HF1 | 73.98 | –4.77 | −0.233 | 0.113 | 0.966 |
| | | –2.31 | −0.471 | 0.856 | –0.213 |
| | | 7.08 | 0.851 | 0.504 | 0.146 |
| HF2 | 9.33 | –5.28 | 0.266 | 0.229 | 0.936 |
| | | –4.24 | 0.244 | –0.956 | 0.164 |
| | | 9.52 | 0.932 | 0.185 | –0.310 |
| S2 | | | | | |
| HF1 | 39.26 | –3.75 | 0.517 | –0.632 | 0.577 |
| | | –3.06 | 0.124 | –0.612 | –0.781 |
| | | 6.81 | 0.847 | 0.475 | –0.238 |

agreement is excellent for the C3′-centered model: the principal directions differ by 7° or less and the anisotropic HF couplings are very similar. The calculated isotropic HF couplings are 5–10 MHz smaller than experimentally observed, as often encountered in such calculations for this type of HF coupling (e.g., see refs. *11, 19*). The vanishing isotropic HFC of the H(O3′) proton in the DFT calculations (predicted splitting of 0.16 mT for B // <b>) is also in agreement with the absence of a corresponding HF splitting in the EIE pattern (Fig. 3). This strongly suggests that I1 is an H-abstracted, C3′-centered radical.

Both HF interactions of I2 are small ($A_{iso}$ <10 MHz), in agreement with the lack of resolved HF structure in the EPR and EIE spectra (Fig. 3). The anisotropy of the HF1(I2) tensor again is typical of a nonexchangable β proton, while that of HF2(I2) is in between typical values for β and γ protons. HF2(I2) is in fact very similar to HF interactions observed for the dominant stable radicals in sucrose (*8, 9*) and for a radical present in glucose 1-phosphate after 77 K irradiation (*13, 14*). These were shown to arise from the γ proton in a $-\dot{C}-(C=O)-CH_{\gamma}-$ or $-\dot{C}-O-CH_{\gamma}-$ structure. Both this observation and the enhanced *g*-tensor anisotropy point to a carbonyl group and/or ring oxygen neighboring the radical center. Taking this into account, and comparing $\vec{V}_{max}$ of HF1 and HF2 with all pristine $C_{\alpha}$—$H_{\beta}$ and $C_{\alpha}$—$H_{\gamma}$ directions, respectively (Supplementary Tables S2 and S4: http://dx.doi.org/10.1667/RR3179.1.S1), we arrived at three plausible model structures ($I2_{M1}$, $I2_{M2}$, $I2_{M3}$), as depicted in Fig. 7. The corresponding DFT proton HF tensors are shown in Supplementary Table S5(http://dx.doi.org/10.1667/RR3179.1.S1) for all three structures and in Table 2 for $I2_{M1}$. The isotropic HF interaction of H(C4′) is too large (>60 MHz) for $I2_{M2}$, as are those of H(C4′) and H'(C6′) (>75 MHz) for model $I2_{M3}$. However, good correspondence is found for $I2_{M1}$ (Table 2); all isotropic HF interactions are less than 15 MHz, the anisotropic HF values show a close resemblance, and the eigenvector deviations are small, especially for the $\vec{V}_{max}$ directions that provide the most crucial criterion. In conclusion, all available evidence points toward I2 being a radical centered at C2 with a carbonyl group at C3.

*Stable species*. Q-band ENDOR spectra of trehalose single crystals after X irradiation at room temperature and subsequent annealing at 40°C for 3 days are shown in Fig. 8. Extensive ENDOR measurements in the *ab*, *bc* and *ac* planes allowed determination of three HF interactions for the stable species (Fig. 9 and Table 1), two for S1, and one for S2. Their anisotropies again indicate that all three originate from nonexchangeable protons in a β position. The isotropic HFC values of HF1(S1) and HF2(S1) (74 MHz and 9 MHz, respectively) are in agreement with the doublet-of-doublets EIE spectrum (Fig. 4). Although for S2

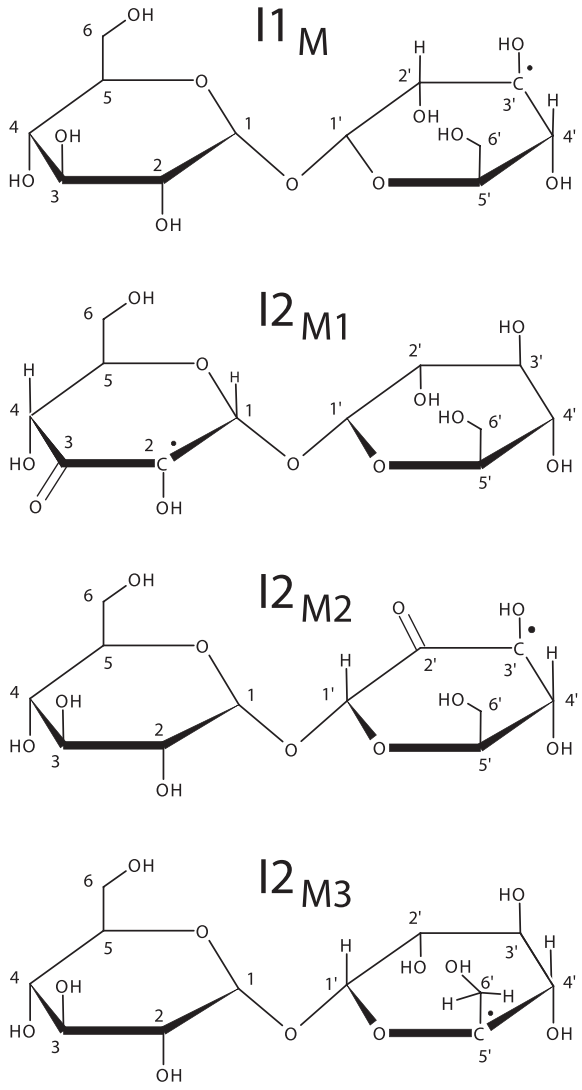


**FIG. 7.** Chemical structures of radical models for I1 and I2. The DFT-calculated HF tensors of these structures are reported in Table 2 and Supplementary Table S5 (http://dx.doi.org/10.1667/RR3179.1.S1). Only those carbon-bound protons for which HF tensors are reported are depicted explicitly.

only one HF tensor [HF1(S2)] could be determined, the EIE spectra (Fig. 4) also point to the presence of an additional smaller HF interaction. There are a few ENDOR lines close to the proton Larmor frequency that we could not assign with certainty to S1 or S2. These may indicate the presence of other (minor) radicals in the stable stage.

Taking into account the requirement of at least two carbon-bound β protons for S1 (and no α proton) and comparing the $\vec{V}_{max}$ principal directions with pristine $C_\alpha$—$H_\beta$ crystal directions (Supplementary Table S2, http://dx.doi.org/10.1667/RR3179.1.S1), we arrive at C2 and C5′ as the most plausible radical $C_\alpha$ centers for S1. The same reasoning for S2, which has at least one carbon-bound β proton, again leads to C2 and C5′, but also C3, C5, C3′ and C4′ are possible centers here. The DFT-calculated HF tensors of the radical species obtained by H abstraction at these carbon atoms are given in Supplementary Table S3 (http://dx.doi.org/10.1667/RR3179.1.S1).

Whereas DFT predicts two big β-HFCs (>75 MHz) for the C5′-centered species, the calculated principal values of HF tensors H(C1) and H(C3) in the C2-centered species ($S1_M$ in Fig. 10 and HF tensors iterated in Table 3) agree well with those of HF2(S1) and HF1(S1), respectively, although the isotropic part of H(C3) is somewhat too large. Furthermore, the calculated H(O2) isotropic HFC of about 0 MHz is in accordance with the fact that it was not detected experimentally: the predicted splitting is 0.27 mT for B // <b> and does not exceed 0.4 mT at the a, b, and c axes, which is within the observed line widths. The principal directions of H(C1) and HF2(S1) also agree well, but those of H(C3) and HF1(S1) show more discrepancies. Notably the deviation of 17° for the $\vec{V}_{max}$ eigenvectors is larger than may be expected for the advanced calculations employed here. Some further improvement can be obtained by limited (constrained) reorientation of the C3-H(C3) bond, but none of our DFT calculations resulted in a truly satisfactory agreement. Also, it appears unlikely that the simple H-abstracted C2-centered species would be stable, considering that I2 (model $I2_{M1}$ in Fig. 7), which additionally has a stabilizing carbonyl group at C3, is not stable. S1 may well be structurally similar to the H-abstracted species centered at C2, but its precise structure remains uncertain.

None of the H-abstracted species mentioned above provide a good model for S2. Most notably, all of them are characterized by at least one β proton with an isotropic HFC of more than 85 MHz, in contrast to the experimental value of 39 MHz for HF1(S2). This has led us to consider radical structures resulting from β elimination, opening of the rings and breaking of the glycosidic bond. A large number of radicals with the unpaired electron at the aforementioned carbon positions can result from such mechanisms, but at present we have not found a model that gives an overall good agreement. The model showing the closest correspondence is shown in Fig. 10 ($S2_M$, HF tensors in Table 3); a C2-centered species with a carbonyl group at C1 and a broken glycosidic bond. Stable radical species with similar characteristics were convincingly identified in sucrose (*8, 9*). The calculated H(C3) and experimental HF1(S2) tensors agree rather well with respect to the $\vec{V}_{max}$ principal direction (deviation of 11°) and the anisotropic HFCs. Also, the magnitude of calculated H(O2) interaction (0.5–0.6 mT for B // <b>) is in agreement with the additional small HF splitting detected experimentally (Fig. 4). However, (1) the other principal directions of H(C3) and HF1(S2) deviate by almost 90°, and (2) the isotropic HFC is considerably overestimated in the calculations [63 MHz for H(C3) vs. 39 MHz for HF1(S2)]. The former discrepancy (which can be interpreted as an interchanging of the two ''axial'' components in the calculation) is not a critical issue, we have observed it in the past for some (well-established) radical models in similar materials and

**TABLE 2**
**DFT-Calculated Proton HF Tensors for Radical Models $I1_M$ and $I2_{M1}$ (Fig. 7)[a]**

| Radical model | Proton | Iso (MHz) | Aniso (MHz) | Principal directions a | b | c | δ (°) HF1(I1) | HF2(I1) |
|---|---|---|---|---|---|---|---|---|
| $I1_M$ | H(C2′) | 87.90 | –5.08 | –0.437 | 0.844 | –0.310 | 7 | |
| | | | –2.49 | –0.855 | –0.497 | –0.147 | 6 | |
| | | | 7.57 | –0.278 | 0.201 | 0.939 | 4 | |
| | H(C4′) | 78.09 | –5.36 | 0.387 | –0.905 | –0.175 | | 6 |
| | | | –1.85 | –0.382 | –0.331 | 0.863 | | 6 |
| | | | 7.21 | –0.839 | –0.267 | –0.474 | | 3 |
| | H(O3′) | 0.58 | –11.28 | 0.918 | –0.196 | 0.344 | | |
| | | | –9.12 | –0.374 | –0.718 | 0.587 | | |
| | | | 20.41 | –0.132 | 0.667 | 0.733 | | |
| | | | | | | | HF1(I2)) | HF2(I2) |
| $I2_{M1}$ | H(C1) | 13.20 | –3.36 | –0.153 | 0.980 | 0.129 | 14 | |
| | | | –2.74 | 0.340 | –0.071 | 0.938 | 14 | |
| | | | 6.10 | 0.928 | 0.187 | –0.323 | 1 | |
| | H(C4) | 10.14 | –2.41 | 0.365 | –0.815 | 0.449 | | 15 |
| | | | –1.60 | –0.905 | –0.197 | 0.377 | | 15 |
| | | | 4.01 | –0.219 | –0.544 | –0.810 | | 3 |
| | H(O2) | 3.05 | –10.23 | 0.443 | –0.217 | –0.870 | | |
| | | | –8.39 | 0.169 | –0.932 | 0.319 | | |
| | | | 18.62 | 0.880 | 0.289 | 0.376 | | |

[a]δ are the deviations between the calculated and the experimental principal directions.

reported it explicitly for a glycine radical (*37*). The latter discrepancy, however, is too large to be attributed to an inherent computational inaccuracy. DFT calculations on different conformations of $S2_M$ and related chemical structures did not result in a better model. Measurements on selectively $^{13}C$ and/or $^{2}H$ enriched samples will probably be necessary to make further progress in the identification of S2.

## DISCUSSION AND CONCLUSIONS

X irradiation at room temperature produces at least three different semistable radical species (I1, I2, I3) in trehalose single crystals. DFT calculations indicate that the two species dominating the initial EPR spectrum (I1 and I2) very likely result from H abstraction at C3′ (I1) and C2 (I2), the latter with the additional formation of a carbonyl group at C3. After 3 months at room temperature or 3 days at

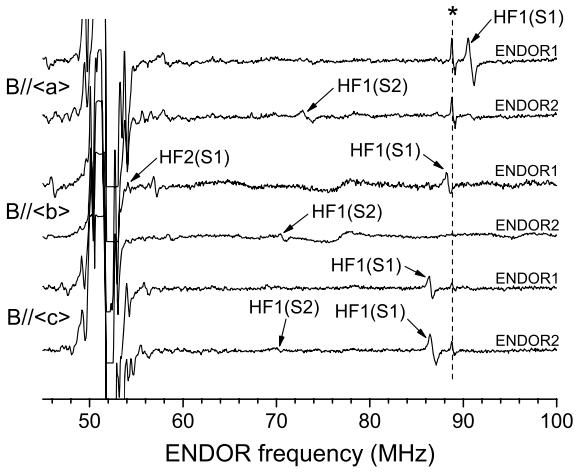


**FIG. 8.** Q-band ENDOR spectra of trehalose single crystals after room-temperature X irradiation and annealing at 40°C for 3 days with the magnetic field oriented along the <a>, <b> and <c> axes. For each orientation, the ENDOR spectra are shown for two different positions in the EPR spectrum, as indicated by arrows for B // <b> in Fig. 4. The signal at 89 MHz (indicated by *) is an artifact.

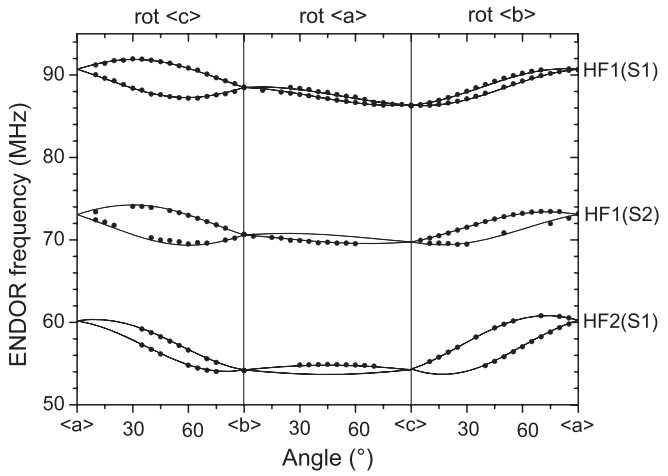


**FIG. 9.** Q-band ENDOR angular variation of proton HF interactions of the stable radical species in room-temperature irradiated trehalose single crystals in the ab, bc and ac planes. The solid circles represent the experimental data of the interactions for which HF tensors were determined and the solid lines are simulations using the HF tensors in Table 1.

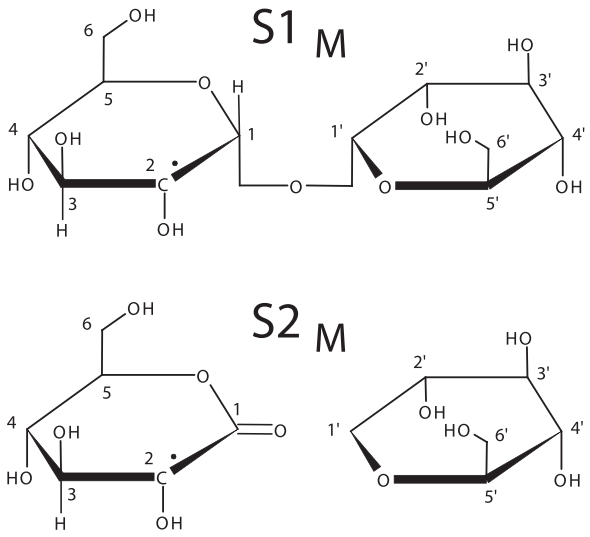


**FIG. 10.** Chemical structures of radical structure models for S1 and S2. The DFT-calculated HF tensors on these structures are reported in Table 3. Only the carbon-bound protons for which HF tensors are reported are depicted explicitly.

40°C, I1 and I2 have decayed and the EPR spectrum is dominated by two other species (S1 and S2). Neither of these species could be identified conclusively, but the available data indicates that S1 is C2-centered.

Gräslund and Löfroth have also conducted a study on the radicals induced in trehalose by irradiation at room temperature (*23*). These authors report an initial stage with only one dominant radical species exhibiting a 1:2:1 triplet EPR signature with a 3 mT splitting (species A), which clearly must correspond to species I1 in our current work. Gräslund and Löfroth attributed this spectrum to H-abstracted species centered at C3 and C3′. Our ENDOR and DFT analysis provides strong indications, based on the fact that the two glucose units have different relative orientations with respect to the crystallographic axes, that only the C3′-centered species is formed in significant amounts. This again demonstrates the regioselectivity of radiation damage, in spite of the (seeming) structural equivalency of the two monosaccharide units. Although these units seem quite symmetric in representations such as Fig. 1B, they have different 3D-conformations in the lattice (e.g., with respect to the relative orientations of the hydroxyl groups) and different local environments, which result in different pathways of radiation damage.

We report two new species I2 and I3 in the current work. Gräslund and Löfroth performed most of their measurements at 77 K after irradiation at 77 K and together with the lower spectral resolution of their X-band experiments this may explain why these species escaped detection in their study.

The general analysis of the stable EPR spectrum (3 months after X irradiation or 3 days after irradiation at 40°C) by Gräslund and Löfroth is in agreement with ours: two dominant species, both with a doublet-of-doublets EPR signature. However, those authors proposed that the larger HF interaction of each radical originates from an α proton, which is in clear contrast to the pure β-type anisotropy of the HF1(S1) and HF1(S2) tensors we observed here. Furthermore, the magnitude of the (isotropic) HFCs does not agree with those in our studies. The most obvious explanation is that Gräslund and Löfroth did not have ENDOR or EIE as their disposal to unravel the composite EPR spectra. Consequently, the structures they put forward (C2- and C2′-centered species with carbonyl group formation at C3 and C3′, respectively, resulting from water elimination reactions of the initial species) likely are incorrect. At any rate, they are in direct disagreement with our experimental observations.

**TABLE 3**
**DFT-Calculated Proton HF Tensors for Radical Models $S1_M$ and $S2_M$ (Fig. 10)[a]**

| | | | | Principal directions | | | δ (°) | |
|---|---|---|---|---|---|---|---|---|
| Radical model | Proton | Iso (MHz) | Aniso (MHz) | a | b | c | HF1(I2) | HF2(I2) |
| $S1_M$ | H(C1) | 12.25 | –5.35 | 0.206 | 0.395 | 0.895 | | 11 |
| | | | –4.12 | 0.266 | –0.903 | 0.337 | | 10 |
| | | | 9.47 | 0.942 | 0.169 | –0.291 | | 2 |
| | H(C3) | 89.26 | –4.70 | –0.300 | 0.323 | 0.898 | 26 | |
| | | | –1.85 | 0.499 | 0.855 | –0.141 | 20 | |
| | | | 6.55 | –0.813 | 0.406 | –0.418 | 17 | |
| | H(O2) | 0.39 | –10.34 | –0.350 | –0.464 | 0.814 | | |
| | | | –9.26 | –0.418 | 0.855 | 0.307 | | |
| | | | 19.59 | –0.838 | –0.233 | –0.493 | | |
| | | | | | | | HF1(S1) | |
| $S2_M$ | H(C3) | 62.82 | –4.12 | –0.100 | 0.622 | 0.776 | 84 | |
| | | | –2.18 | –0.543 | –0.688 | 0.481 | 84 | |
| | | | 6.30 | 0.833 | –0.374 | 0.407 | 11 | |
| | H(O2) | −7.67 | –8.84 | 0.269 | –0.889 | –0.371 | | |
| | | | –7.36 | 0.418 | 0.455 | –0.786 | | |
| | | | 16.20 | 0.867 | 0.056 | 0.494 | | |

[a]δ are the deviations between the calculated and the experimental principal directions.

A final comment on the article by Gräslund and Löfroth concerns the identity of the radicals stabilized after X irradiation at 77 K. Since the EPR spectrum looks quite similar to that observed initially after X-irradiation at room temperature (also dominated by a 1:2:1 triplet with a ~3 mT splitting), these authors concluded that the same (dominant) species are present at both stages. However, a previous ENDOR and DFT analysis in our laboratories convincingly showed that the triplet at 77 K originates from an H-abstracted C4-centered species (*20*). In addition, we show here that the triplet in the initial stage after room-temperature irradiation can be attributed to an H-abstracted C3′-centered species. It is interesting to note that the EPR spectrum after X irradiation at 10 K is also dominated by a triplet, which could be attributed to yet another H-abstracted species, centered at C5′ (*19*). This illustrates the need for caution when interpreting composite EPR spectra and emphasizes the risk of identifying radical structures and reaction mechanisms without detailed analysis by ENDOR and advanced quantum chemical calculations.

Recently, we demonstrated that the 3 dominant stable radicals in sucrose single crystals are characterized by a broken glycosidic bond and carbonyl groups (*8, 9*). Similar characteristics were found for the dominant radical in glucose 1-phosphate after 77 K irradiation (*13, 14*). The structure of the initial I2 species proposed here provides further proof that carbonyl group formation indeed is a common radiation-induced process in sugar compounds. S2 may result from glycosidic bond scission, but no clear evidence for this process has been obtained in the present study. Remarkably, the most dominant initial species appears to result from a simple net H-abstraction. Two such species (C3- and C6-centered) have also been shown to be stable in X-irradiated glucose (*38–40*). Investigation of the free radicals induced by X-irradiation in other disaccharides is necessary to obtain insight into these discrepancies and similarities.

In the current study and in previous papers published by our laboratories (*19, 20*), we have carefully investigated the radiation-induced radicals in trehalose single crystals at four different stages: after irradiation at 10 K and 77 K, and in the initial and stable state after irradiation at room temperature. Ideally, this information should allow us to devise reaction chains linking the (more) primary species to those that are stable. However, the myriad of radicals present at lower temperature make this a formidable task as does the decay in total intensity (observed between any two consecutive stages for trehalose), which points to the conversion of radicals into diamagnetic species. This decay is in fact observed for many thermally induced EPR spectral changes in the case of radicals, and poses a significant problem for reliably establishing chemical pathways altogether. The initial and stable spectra after room-temperature irradiation appear somewhat less complex. However, the structures of S1 and S2 are uncertain. Even if S1 is assumed to be a simple H-abstracted C2-centered species, there are no obvious single-step reaction paths leading from I1 or I2 to S1. Careful and extensive annealing experiments at intermediate temperatures, extended with spectral simulations, would be necessary to reliably map the radiation chemistry for trehalose, which is beyond the scope of the current work.

Finally, it is interesting that the unpaired electron localized at the C2 carbon in I2, quite likely also in S1 and possibly in S2 as well. Similarly, four out of 6 observed stable radicals in fructose after room-temperature irradiation appear to be C3-centered (*2*). This again indicates that specific sites in a molecule are more efficient at trapping stable radicals, although no obvious explanation has yet emerged for this selectivity.

## ACKNOWLEDGMENT

The authors, De Cooman and Tarpan wish to acknowledge the Fund for Scientific Research, Flanders (Belgium) (F.W.O.-Vlaanderen) for financial support.

Received: August 30, 2012; accepted: November 8 2012; published online: February 1, 2013

## REFERENCES

1. Tarpan MA, Sagstuen E, Pauwels E, Vrielinck H, Waroquier M, Callens F. Combined electron magnetic resonance and density functional theory study of 10 K X-irradiated beta-D-Fructose single crystals. J Phys Chem A 2008; 112:3898–905.
2. Tarpan MA, Vrielinck H, De Cooman H, Callens F. Determination of the g tensors for the dominant stable radicals in X-irradiated beta-D-fructose single crystals. J Phys Chem A 2009; 113:7994–8000.
3. Vanhaelewyn G, Lahorte P, De Proft F, Mondelaers W, Geerlings P, Callens F. Electron magnetic resonance study of stable radicals in irradiated D-fructose single crystals. Phys Chem Chem Phys 2001; 3:1729–35.
4. Vanhaelewyn GCAM, Pauwels E, Callens FJ, Waroquier M, Sagstuen E, Matthys PFAE. Q-band EPR and ENDOR of low temperature X-irradiated beta-D-fructose single crystals. J Phys Chem A 2006; 110:2147–56.
5. Vanhaelewyn GCAM, Jansen B, Pauwels E, Sagstuen E, Waroquier M, Callens FJ. Experimental and theoretical electron magnetic resonance study on radiation-induced radicals in alpha-L-sorbose single crystals. J Phys Chem A 2004; 108:3308–14.
6. Pauwels E, Van Speybroeck V, Vanhaelewyn G, Callens F, Waroquier M. DFT-EPR study of radiation-induced radicals in alpha-D-glucose. Int J Quantum Chem 2004; 99:102–8.
7. De Cooman H, Pauwels E, Vrielinck H, Dimitrova A, Yordanov N, et al. Radiation-induced defects in sucrose single crystals, revisited: A combined electron magnetic resonance and density functional theory study. Spectrochim Acta A 2008; 69:1372–83.
8. De Cooman H, Pauwels E, Vrielinck H, Sagstuen E, Callens F, Waroquier M. Identification and conformational study of stable radiation-induced defects in sucrose single crystals using density functional theory calculations of electron magnetic resonance parameters. J Phys Chem B 2008; 112:7298–307.
9. De Cooman H, Pauwels E, Vrielinck H, Sagstuen E, Van Doorslaer S, et al. ENDOR and HYSCORE analysis and DFT-assisted identification of the third major stable radical in sucrose single crystals X-irradiated at room temperature. Phys Chem Chem Phys 2009, 11:1105–14.
10. Vrielinck H, De Cooman H, Karakirova Y, Yordanov ND, Callens

F. Early-stage evolution of the EPR spectrum of crystalline sucrose at room temperature after high-dose X irradiation. Radiat Res 2009; 172:226–33.

*11*. De Cooman H, Pauwels E, Vrielinck H, Sagstuen E, Waroquier M, Callens F. Oxidation and reduction products of X irradiation at 10 K in sucrose single crystals: radical identification by EPR, ENDOR, and DFT. J Phys Chem B 2010; 114:666–74.

*12*. Vanhaelewyn G, Sadlo J, Callens F, Mondelaers W, De Frenne D, Matthys P. A decomposition study of the EPR spectrum of irradiated sucrose. Appl Radiat Isotopes 2000; 52:1221–7.

*13*. De Cooman H, Vanhaelewyn G, Pauwels E, Sagstuen E, Waroquier M, Callens F. Radiation-induced radicals in glucose-1-phosphate. I. Electron paramagnetic resonance and electron nuclear double resonance analysis of in situ X-irradiated single crystals at 77 K. J Phys Chem B 2008; 112:15045–53.

*14*. Pauwels E, De Cooman H, Vanhaelewyn G, Sagstuen E, Callens F, Waroquier. M. Radiation-induced radicals in glucose-1-phosphate. II. DFT analysis of structures and possible formation mechanisms. J Phys Chem B 2008; 112:15054–63.

*15*. Bernhard WA, Close DM. DNA damage dictates the biological consequences of ionizing irradiation: The chemical pathways. In: Mozumder A, Hatano Y, editors. Charged particle and photon interactions with matter: Chemical, physicochemical, and biological consequences with applications. New York: Marcel Dekker; 2003. P. 1–470.

*16*. Becker D, Adhikary A, Sevilla MD. The role of charge and spin migration in DNA radiation damage. In: Chakraborty T, editor. Charge migration in DNA physics, chemistry and biology perspectives. Berlin, Heidelberg: Springer-Verlag; 2007. P. 9–175.

*17*. Sagstuen E, Hole EO. Radiation produced radicals. In: Brustolon M, Giamello E, editors. Electron paramagnetic resonance: A practitioner's toolkit. Hoboken (NJ): Wiley & Sons, Inc.; 2008. P. 325–82.

*18*. Karakirova Y, Yordanov ND, De Cooman H, Vrielinck H, Callens F. Dosimetric characteristics of different types of saccharides: An EPR and UV spectrometric study. Radiat Phys Chem 2010; 79: 654–9.

*19*. Tarpan MA, De Cooman H, Sagstuen E, Waroquier M, Callens F. Identification of primary free radicals in trehalose dihydrate single crystals X-irradiated at 10 K. Phys Chem Chem Phys 2011; 13:11294–302.

*20*. Tarpan MA, De Cooman H, Hole EO, Waroquier M, Callens F. Radiation products at 77 K in trehalose single crystals: EMR and DFT analysis. J Phys Chem A 2012; 116:3377–87.

*21*. Samskog PO, Kispert LD, Lund A. Geometric model of trapped electrons in trehalose single crystals x-ray irradiated at 3 K. An EPR study. J Chem Phys 1983; 78: 5790–4.

*22*. Samskog PO, Kispert LD, Lund A. An ESR study of 77 K alkoxy and hydroxyalkyl radicals in x-ray irradiated trehalose single crystals. J Chem Phys 1982; 77:2330–5.

*23*. Gräslund A, Löfroth G. Free-radicals in gamma-irradiated single-crystals of trehalose dihydrate and sucrose studied by electron-paramagnetic resonance. Acta Chem Scand B 1975; 29:475–82.

*24*. Derbyshire W. The coupling between an unpaired electron spin and a proton two bonds away. Mol Phys 1962; 5:225–31.

*25*. Heller C, McConnell HM. Radiation damage in organic crystals .2. Electron spin resonance of (CO2H)CH2CH(CO2H) in beta-succinic acid. J Chem Phys 1960; 32:1535–9.

*26*. Brown GM, Rohrer DC, Berking B, Beevers CA, Gould RO, Simpson R. Crystal structure of alpha,alpha-trehalose dihydrate from 3 independent X-ray determinations. Acta Crystallog B 1972; B 28:3145–58.

*27*. Schonland DS. On the determination of the principal g-values in electron spin resonance. P Phys Soc Lond 1959; 73:788–92.

*28*. Vrielinck H, De Cooman H, Tarpan MA, Sagstuen E, Waroquier M, Callens F. Schonland ambiguity in the electron nuclear double resonance analysis of hyperfine interactions: Principles and practice. J Magn Reson 2008, 195:196–205.

*29*. Declerck R, Van Speybroeck V, Waroquier M. First-principles calculations of hyperfine parameters with the Gaussian and augmented-plane-wave method: Application to radicals embedded in a crystalline environment. Phys Rev B 2006, 74: 245103(8).

*30*. Lippert G, Hutter J, Parrinello M. The Gaussian and augmented-plane-wave density functional method for ab initio molecular dynamics simulations. Theor Chem Acc 1999, 103: 124–140.

*31*. Becke AD. Density-functional exchange-energy approximation with correct asymptotic behavior. Phys Rev A 1988, 38: 3098–100.

*32*. Lee CT, Yang WT, Parr RG. Development of the Colle-Salvetti correlation-energy formula into a functional of the electron density. Phys Rev B 1988, 37:785–9. http://cp2k.berlios.de.

*33*. Sagstuen E, Lund A, Awadelkarim O, Lindgren M, Westerling J. Free-radicals in X-irradiated single-crystals of sucrose–a reexamination. J Phys Chem 1986; 90:5584.

*34*. Ko C-L, Box HC. Exchangeable proton couplings in free-radicals – radiation products of hydroxypyroline HCL. J Chem Phys 1978; 68:5357–62.

*35*. Muto H, Nunome K, Iwasaki M. ENDOR studies of super-hyperfine couplings of hydrogen-bonded protons .2. Protonated radical-anion in irradiated succinic acid single-crystals. J Chem Phys 1974; 61:1075–7.

*36*. Pauwels E, Van Speybroeck V, Waroquier M. Evaluation of different model space approaches based on DFT to examine the EPR parameters of a radiation-induced radical in solid-state a-glycine. J Phys Chem A 2004; 108:11321–32.

*37*. Madden KP, Bernhard WA. ESR-ENDOR study of X-irradiated single crystals of alpha-methyl-D-glucopyranoside. J Chem Phys 1979; 70:2431–7.

*38*. Madden KP, Bernhard WA. Thermally induced free-radical reactions in alpha-D-glucopyranose single-crystals–an electron-spin resonance-electron nuclear double-resonance study. J Phys Chem 1982; 86:4033–6.

*39*. Pauwels E, Van Speybroeck V, Waroquier M. Radiation-induced radicals in alpha-D-glucose: Comparing DFT cluster calculations with magnetic resonance experiments. Spectrochim Acta A 2006; 63:795–801.